
SATORI-R1: Incentivizing Multimodal Reasoning with Spatial Grounding and Verifiable Rewards

Chuming Shen¹, Wei Wei^{1*}, Xiaoye Qu¹, Yu Cheng²

¹ School of Computer Science & Technology, Huazhong University of Science and Technology

² The Chinese University of Hong Kong

{scm, weiw, xiaoye}@hust.edu.cn chengyu@cse.cuhk.edu.hk

Abstract

DeepSeek-R1 has demonstrated powerful reasoning capabilities in the text domain through stable reinforcement learning (RL). Recently, in the multimodal domain, works have begun to directly apply RL to generate R1-like free-form reasoning for Visual Question Answering (VQA) tasks. However, multimodal tasks share an intrinsically different nature from textual tasks, which heavily rely on the understanding of the input image to solve the problem. Therefore, such free-form reasoning faces two critical limitations in the VQA task: (1) Extended reasoning chains diffuse visual focus away from task-critical regions, degrading answer accuracy. (2) Unverifiable intermediate steps amplify policy-gradient variance and computational costs overhead. To address these issues, in this paper, we introduce SATORI (Spatially Anchored Task Optimization with ReInforcement Learning), which decomposes VQA into three verifiable stages, including global image captioning, region localization, and answer prediction, each supplying explicit reward signals. Furthermore, we also introduce VQA-Verify, a 12k dataset annotated with answer-aligned captions and bounding-boxes to facilitate training. Experiments demonstrate consistent performance improvements across seven VQA benchmarks, achieving up to 15.7% improvement in accuracy compared to the R1-like baseline. Our analysis of the attention map confirms enhanced focus on critical regions, which brings improvements in accuracy. Our code is available at <https://github.com/justairr/SATORI-R1>.

1 Introduction

The recent surge of interest in models such as DeepSeek-R1 [14, 48] has sparked renewed attention toward using reinforcement learning (RL) as a direct training strategy for reasoning models [63, 33, 73, 51, 69]. Inspired by these advances, in the realm of multimodal tasks, particularly Visual Question Answering (VQA), prevailing approaches [22, 33, 44] draw inspiration from the RL paradigm widely adopted in language models. This approach encourages models to first generate a verbose reasoning pattern, akin to “free-form exploration”, before producing a final answer [14, 48, 56, 60, 52]. While such reflection can benefit multi-hop or abstract reasoning tasks by promoting systematic knowledge retrieval and decomposition, it reveals fundamental limitations when applied to standard VQA tasks.

Specifically, there are two key limitations in applying R1-like reasoning patterns to standard VQA tasks: (1) Attention Dilution in Critical Regions: Free-form reasoning patterns tend to diffuse the model’s focus away from task-relevant visual areas. As a result, the visual attention maps exhibit lower density over regions that are essential for answering the question. By comparing attention distributions across several reinforcement-learning training paradigms, we observe that when the

* Corresponding authors.

model generates long reasoning chains, it reallocates attention to irrelevant elements in the scene. This dispersion significantly degrades VQA performance. (2) Convergence Impediment [15, 77]: Unstructured reasoning paths not only multiply token consumption but also, in the absence of quantifiable intermediate supervisory verifiable signals, induce high variance in the policy-gradient estimates, thereby slowing convergence. Under standard RL configurations, each training example must undergo multiple rollouts to accurately evaluate an extended reasoning trajectory, which further inflates computational overhead. Consequently, scalable training becomes impractical in environments with limited resources.

To bridge these gaps, we introduce **SATORI** (Spatially Anchored Task Optimization with Reinforcement Learning), a new visual reinforcement learning paradigm that incorporates verifiable reasoning patterns. Previous works [47, 4] have demonstrated that pre-outputting an overall image caption and the critical region yields significant improvements in VQA tasks, and both of them are easy to verify. This motivates us to have the model first generate an image caption to capture the entire scene and establish a global understanding, then produce key bounding-boxes to shift visual attention to regions relevant to the question, and finally formulate an answer based on this focused information. We employ image caption and bounding-box as verifiable reasoning patterns, followed by reinforcement learning to directly train the model.

To facilitate the training of our above proposed paradigm, we introduce VQA-Verify, the first multi-modal VQA dataset with both bounding-box and caption annotations. It comprises 12k samples from 17 benchmarks, structured hierarchically into 3 categories, Perception, Reasoning, and Multilingual, and 11 fine-grained task classes. Each entry includes an image, question, answer, a bounding-box highlighting the answer cue, and a concise caption describing the image.

SATORI offers two key advantages: (1) Sharper Attention Alignment: Through analysis of the visual attention maps generated by MLLMs, our method focuses more on critical regions compared to typical R1-like reasoning patterns, thereby improving accuracy in visual question answering (VQA). (2) Verifiable Intermediate Rewards: During the reinforcement learning process, our newly designed reward provides a *smooth* approximation of the VQA accuracy reward, reducing policy-gradient variance by 27%. We conduct evaluations across seven VQA benchmarks, demonstrating that **SATORI** achieves state-of-the-art performance among models with 3B parameters, improving MMBench [29] accuracy by an absolute 15.7% over the base model and surpassing comparable methods on mathematical reasoning tasks by 4.6 to 9.0 points.

To summarize, our key contributions are:

- We analyze MLLM attention maps and show that free-form reasoning dilutes focus on answer-relevant regions, motivating more targeted intermediate steps.
- We propose a three-step visual reasoning pattern and RL paradigm **SATORI**. By turning caption and localization into verifiable reward signals, our RL paradigm lowers policy-gradient variance by 27% and speeds up convergence.
- We release VQA-Verify, the first augmented dataset of 12k VQA samples with answer-relevant bounding-boxes and scene captions to enable explicit supervision for our rewards.
- Our method outperforms traditional R1-like free-form reasoning on four comprehensive benchmarks, achieving up to 15.7% improvement in accuracy.

2 Background

2.1 MLLM Architecture and Visual Attention

Multimodal Large Language Models (MLLMs) unify visual and textual reasoning through a hybrid architecture. Given an input image $\mathbf{I} \in \mathbb{R}^{H \times W \times C}$, a vision encoder (e.g., ViT [9]) partitions it into $p \times p$ patches, linearly projected into visual tokens $\{\mathbf{v}_i\}_{i=1}^{N_I}$ with $N_I = \frac{HW}{p^2}$. These tokens reside in the same latent space as text tokens $\{\mathbf{t}_j\}_{j=1}^{N_T}$ from language models like Qwen [2] or Llama [12].

The fused sequence $[\mathbf{v}_1, \dots, \mathbf{v}_{N_I}; \mathbf{t}_1, \dots, \mathbf{t}_{N_T}]$ is processed by transformer decoder layers using masked multi-head self-attention (MHSA). For each layer, the attention operation computes:

$$\text{Attention}(\mathbf{Q}, \mathbf{K}, \mathbf{V}) = \text{softmax}\left(\frac{\mathbf{Q}\mathbf{K}^\top}{\sqrt{d}}\right)\mathbf{V}, \quad (1)$$

where \mathbf{Q} , \mathbf{K} , \mathbf{V} are projections of the input sequence. During auto-regressive answer generation, the query \mathbf{Q}_A for each answer token attends to both visual and textual contexts through:

$$\mathbf{A} = \left[\text{softmax} \left(\frac{\mathbf{Q}_A \mathbf{K}^\top}{\sqrt{d}} \right) \right]_{L,K} \in \mathbb{R}_+^{L \times K \times N_A \times N}, \quad (2)$$

where L and K denote the number of layers and attention heads, respectively.

To analyze visual grounding, we isolate attention weights over visual tokens by reshaping \mathbf{A} into spatial dimensions (h, w) , then aggregate multi-head/layer responses:

$$\tilde{\mathbf{A}} = \text{Normalize} \left(\frac{1}{LK} \sum_{l,k} \mathbf{A}_{l,k} \right) \in \mathbb{R}_+^{h \times w}. \quad (3)$$

2.2 Group Relative Policy Optimization (GRPO)

Group Relative Policy Optimization (GRPO) [48] is a reinforcement learning algorithm that optimizes sequence-generating models without an explicit critic network. For each input q , the current policy $\pi_{\theta_{\text{old}}}$ samples a group of G candidate outputs $\{o_1, \dots, o_G\}$. Each output o_i receives a reward $r_i = R(q, o_i)$, and GRPO directly incorporates clipping and KL-regularization into its objective:

$$\begin{aligned} \mathcal{J}_{GRPO}(\theta) = & \mathbb{E}[q \sim P(Q), \{o_i\}_{i=1}^G \sim \pi_{\theta_{\text{old}}}(O|q)] \\ & \frac{1}{G} \sum_{i=1}^G \frac{1}{|o_i|} \sum_{t=1}^{|o_i|} \left\{ \min \left[h_{i,t} \hat{A}_{i,t}, \text{clip} \left(h_{i,t}, 1 - \varepsilon, 1 + \varepsilon \right) \hat{A}_{i,t} \right] - \beta \text{D}_{KL} [\pi_\theta || \pi_{\text{ref}}] \right\}, \end{aligned} \quad (4)$$

where $h_{i,t} = \frac{\pi_\theta(o_{i,t}|q, o_{i,<t})}{\pi_{\theta_{\text{old}}}(o_{i,t}|q, o_{i,<t})}$ and $\hat{A}_{i,t}$ is the (possibly standardized) advantage at step t . This formulation blends the clipped importance-sampling term with a KL-penalty to keep the updated policy close to the reference π_{ref} .

3 SATORI

In this section, we first analyze the visual attention maps of the MLLM, demonstrating that different reasoning patterns influence the model’s focus on critical regions and that spatial reasoning patterns enhance attention to key areas (Section 3.1). Next, we examine the impact of introducing verifiable reasoning patterns on gradient variance during the RL process (Section 3.2). Finally, we propose a visual reinforcement learning paradigm that incorporates verifiable reasoning patterns (Section 3.3).

3.1 Spatial Reasoning Patterns Enhance Attention to Critical Regions

Previous studies [75, 65] demonstrate that attention patterns in MLLM implicitly reflect visual regions critical to task, where localized attention spikes often correlate with image areas relevant to answer. Some studies have attempted to enhance these regions to improve model performance, indicating that attention to critical regions has a significant impact on VQA performance [65]. However, we find that inference patterns based on free-form reasoning tend to weaken the model’s focus on critical regions. This motivates us to explore new forms of reasoning that can guide the model to more accurately attend to image regions relevant to the question, thereby improving VQA performance.

To quantify the differences in attention distributions under three distinct reasoning paradigms, we randomly sampled 2,000 images from the OpenImages [23] dataset and applied the following inference patterns without any fine-tuning: Conventional VQA, free-form reasoning, and Caption-BBox-Answer. These three represent the inference patterns of the original model, the reasoning-enhanced model, and our proposed method, respectively. As illustrated in Figure 1, we ensured a fair comparison by swapping only the output pipeline and employing a one-shot exemplar to steer the model toward each required format.

For each generated answer token, we extract the visual attention weights from all layers and heads, and aggregate them into an $h \times w$ grid to obtain the normalized spatial attention distribution A . More

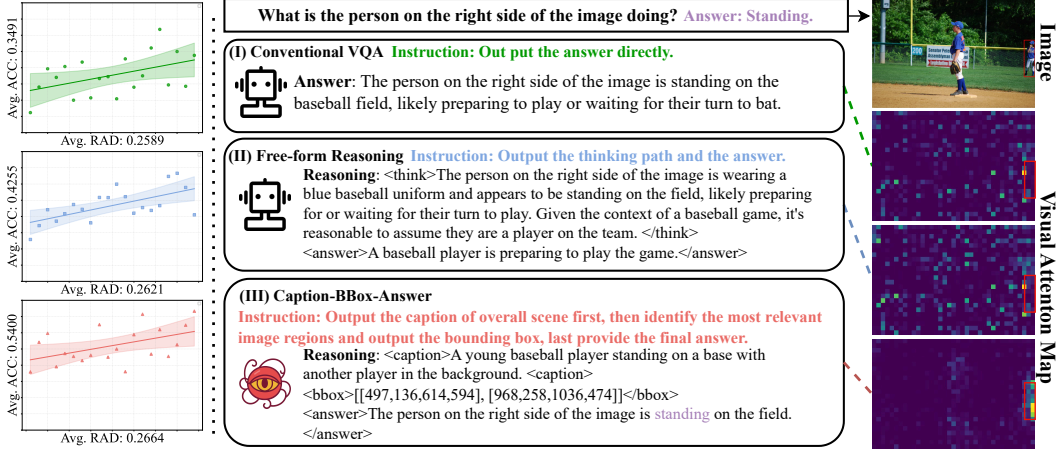


Figure 1: **Left:** The average accuracy and RAD of three different reasoning patterns. **Middle:** An example of different reasoning patterns for the same question. **Right:** A visual example illustrates the differences in attention to key image regions across various inference modes. Using the same model Qwen2.5-VL-Instruct-3B with only the output patterns altered, we observe that compared to other inference approaches, our method enables the model to focus more effectively on the critical regions. The critical regions in the ground truth are marked with red bounding-boxes.

details could be found at Appendix B. Experimental results in Figure 1 show that the attention under the Free-Form setting is more dispersed, whereas the Caption-BBox-Answer setting clearly focuses on regions relevant to the question. Our analysis reveals a critical dependency on *thinking paths*: different reasoning strategies yield distinct attention distributions. As visualized in Figure 1, R1-like free-form reasoning (middle) produces scattered attention patterns across decoder layers, with less attention mass concentrated on critical regions. This phenomenon may be attributed to the fact that regular VQA tasks typically do not require complex chains of reasoning, in contrast to the success of free-form reasoning in more complex mathematical problems. This "overthinking" phenomenon allows the model to hallucinate irrelevant visual features, ultimately diverting focus from semantically salient areas. In contrast, spatial reasoning patterns (bottom) demonstrate layer-consistent attention alignment with human annotations.

This misalignment motivates our quantification framework measuring *Region Attention Density (RAD)*:

$$\text{RAD} = \frac{\sum_{(i,j) \in \mathcal{G}} \tilde{\mathbf{A}}_{i,j}}{\sum_{i=1}^h \sum_{j=1}^w \tilde{\mathbf{A}}_{i,j}} \quad (5)$$

where \mathcal{G} is the set of ground truth bounding-boxes. RAD measures the model's attention to critical regions by calculating the concentration of the attention map within \mathcal{G} . In Figure 2, free-form reasoning patterns exhibit degraded RAD performance due to dispersed attention, whereas our structured *caption-bbox-answer* paradigm maintains higher RAD values, with average scores of 0.2621 and 0.2664, respectively. The results also indicate a positive correlation between RAD and accuracy. More details can be found in Appendix B.

Compared to free-form reasoning, spatially anchored reasoning patterns are also more verifiable and thus better suited as reward signals.

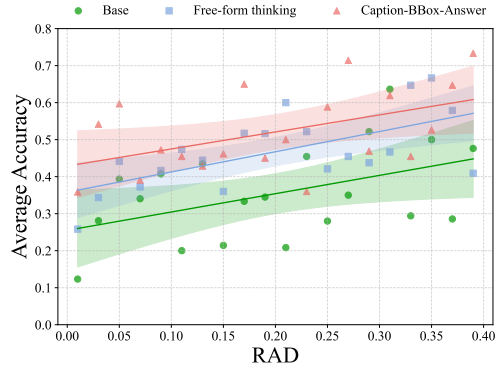


Figure 2: RAD and accuracy distributions for three different reasoning types. The light-shaded region represents the 95% confidence interval.

3.2 Gradient Variance Reduction via Verifiable Reasoning Patterns

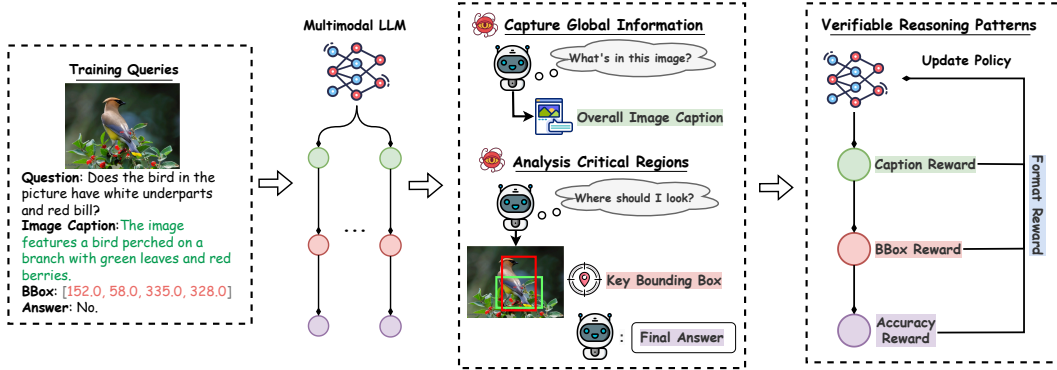


Figure 3: The overview of our proposed method. SATORI guides the model to capture the global information, then analyzes critical regions and finally produces an answer, providing verifiable rewards for step-by-step supervision.

Previous studies [72, 48] have demonstrated that combining verifiable reasoning paths with reinforcement learning (RL) yields strong performance on tasks such as mathematical problem solving and logical inference. This success is largely attributed to the availability of well-structured, deterministic reasoning paradigms that allow for step-by-step supervision. In contrast, open-ended visual reasoning tasks such as VQA present significantly higher uncertainty: the reward signals are sparse, the answers are short, and intermediate reasoning steps are typically not explicitly supervised.

These characteristics introduce substantial variance in the estimation of the policy gradient, which poses a major challenge to effective learning [15, 77]. In particular, token-level policy gradient methods like GRPO rely on sampled trajectories to estimate gradients, where each trajectory receives a global reward that is distributed uniformly across all tokens. Without verifiable intermediate signals, this global reward is highly variable and often lacks sufficient granularity to guide learning effectively.

Motivated by this issue, we aim to reduce the variance of policy gradients by introducing reasoning patterns that are more stable and verifiable. Instead of relying solely on free-form text reasoning, which is difficult to evaluate and highly stochastic, we design our method to incorporate intermediate reasoning steps that can be evaluated through deterministic criteria. This strategy provides a foundation for smoother gradient estimation, which we analyze in detail in Appendix D.

3.3 Spatially Anchored Task Optimization with Reinforcement Learning

As stated in Section 3.1, we propose a structured and verifiable reasoning pattern that aligns with the intrinsic requirements of VQA. Specifically, we replace the free-form reasoning with a caption focusing on the overall image and a bounding-box highlighting the key region. This structured supervision bridges the semantic gap between free-form reasoning and visual grounding requirements. **SATORI** (Spatially Anchored Task Optimization with **Re**inforcement Learning) guides the model to capture both the overall image context and the critical regions before answering the question, providing verifiable rewards for step-by-step supervision. Figure 3 clearly presents the information flow and reward allocation from Caption to BBox to Answer. VQA-Verify enables direct computation of two verifiable reward signals during RL training:

$$\mathcal{R}_{\text{caption}} = \frac{1}{2} (\text{BLEU-4}_{\text{smooth}} + \text{ROUGE-L}_{\text{F1}}), \quad \mathcal{R}_{\text{bbox}} = \text{Union IoU}(\mathcal{P}, \mathcal{G}) \quad (6)$$

where \mathcal{P} is the set of predicted boxes and \mathcal{G} is the set of ground-truth bound boxes. The caption reward $\mathcal{R}_{\text{caption}}$ combines smoothed BLEU-4 (handling zero n-gram matches via additive smoothing) with ROUGE-L F1 (measuring the longest common subsequence overlap). Since there may be multiple bounding-boxes in the ground-truth, we define the Union IoU to compute the intersection over union of the combined bounding-boxes in the image. The detailed calculation process can be found in Algorithm 1. Similar to the R1-like reasoning training method, we also sample two types of reward signals during training: the accuracy reward R_{acc} and the format reward R_{format} . The accuracy reward R_{acc} measures whether the generated answer matches the ground-truth, while the format

reward R_{format} ensures that the output follows the expected format of $\langle \text{caption-BBox-answer} \rangle$. Both reward signals take binary values of 0 or 1.

Algorithm 1 Union IoU Reward Computation

Require: Predicted boxes: $\mathcal{P} = \{B_i^p\}_{i=1}^{N_p}$ where $B_i^p = [x_1^i, y_1^i, x_2^i, y_2^i]$

Ground-truth boxes: $\mathcal{G} = \{B_j^g\}_{j=1}^{N_g}$ where $B_j^g = [x_1^j, y_1^j, x_2^j, y_2^j]$

Ensure: IoU score: $\mathcal{R}_{\text{bbox}} \in [0, 1]$

Convert boxes to geometric polygons:

$$\begin{cases} \mathcal{P}_{poly} = \bigcup_{i=1}^{N_p} \text{Rect}(x_1^i, y_1^i, x_2^i, y_2^i) \\ \mathcal{G}_{poly} = \bigcup_{j=1}^{N_g} \text{Rect}(x_1^j, y_1^j, x_2^j, y_2^j) \end{cases}$$

▷ $\text{Rect}(a, b, c, d)$: Axis-aligned rectangle defined by coordinates (a, b) and (c, d) .

Compute union regions: $\begin{cases} \mathcal{U}_p = \text{Union}(\mathcal{P}_{poly}) \\ \mathcal{U}_g = \text{Union}(\mathcal{G}_{poly}) \end{cases}$

Calculate intersection and union areas: $\begin{cases} A_{\cap} = \text{Area}(\mathcal{U}_p \cap \mathcal{U}_g) \\ A_{\cup} = \text{Area}(\mathcal{U}_p \cup \mathcal{U}_g) \end{cases}$

Compute final IoU with numerical stability: $\mathcal{R}_{\text{bbox}} = \frac{A_{\cap}}{A_{\cup} + \epsilon}$ ($\epsilon = 10^{-6}$)

Subsequently, we guide the model within the prompt to first reason about the image caption and the key region bounding-box, and optimize the prompt solely using the GRPO paradigm. Compared to SFT, which simply imitates annotated data, this training approach leverages policy gradients to encourage the model to explore better generation strategies. By employing independent reward functions for each subtask, the model receives explicit feedback to optimize final accuracy. Similar to the setup in GRPO, we also adopt the basic format reward and accuracy reward.

4 VQA-Verify Dataset

To address the scarcity of explicit visual supervision in VQA training, we introduce VQA-Verify, an small size augmented dataset providing verifiable grounding signals for 12,000 samples across standard VQA benchmarks. Different from standard VQA datasets, VQA-Verify provides annotations for each sample in the form of (Image, Question, Caption, BBox, Answer). To the best of our knowledge, VQA-Verify is the first multimodal dataset that annotates bounding-box and image caption for the answers.

Inspired by previous works [29, 5], VQA-Verify integrates 17 benchmark datasets through a hierarchical framework designed to address diverse visual-textual understanding capabilities. At the highest level, the dataset spans three primary categories: **Perception**, **Reasoning**, and **Multilingual** tasks.

Perception. This category focuses on foundational visual-textual recognition through two subcategories. Document Text Recognition is supported by SROIE [16], which specializes in scanned receipt OCR and key information extraction. Scene Text Recognition encompasses six datasets: Total-Text [7] for multi-oriented and curved text, ICDAR 2013 [20] and ICDAR 2015 [21] as standard benchmarks for horizontal and scene text detection, CTW1500 [30] for curved text analysis, and COCO-Text [58] for text detection in complex scenes. Object Recognition and Detection integrates CUB-200 [59] for fine-grained bird classification and OpenImages [23] for large-scale object detection with bounding-boxes and visual relationships.

Reasoning. This category targets advanced cognitive tasks through six subdomains. Scene Text-based VQA leverages TextVQA [50] for question an-

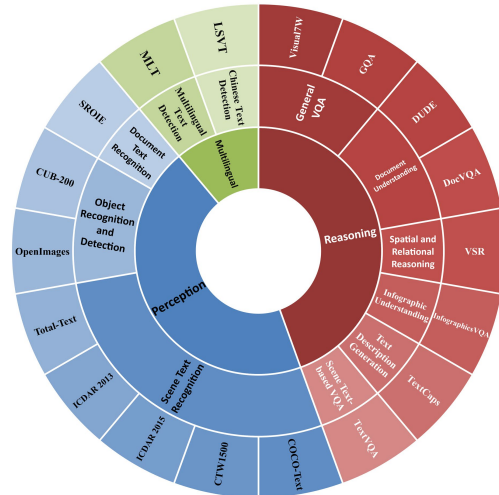


Figure 4: Overview of VQA-Verify. VQA-Verify is divided into 3 categories, 11 subtasks, and 17 benchmarks in total.

swering requiring textual reasoning in images, while Text Description Generation uses TextCaps [49] to challenge models in generating context-aware captions that fuse text and visual elements. Document Understanding combines DocVQA [38] and DUDE [57] to evaluate multi-page document comprehension and layout-aware reasoning. Infographic Understanding employs InfographicVQA [39] to test joint analysis of graphical layouts, data visualizations, and textual content. General VQA integrates GQA [17] for balanced question-answering with scene graph support and Visual7W [82] for object-grounded multimodal QA. Lastly, Spatial and Relational Reasoning incorporates VSR [26] to assess spatial relation verification between objects.

Multilingual. This category includes LSVT [54] for Chinese text detection in street-view scenarios and MLT [40] for script-agnostic text detection across diverse languages. This hierarchical integration provides a unified framework for evaluating both fundamental perception skills and sophisticated reasoning abilities across monolingual and cross-lingual contexts, while maintaining alignment with real-world visual-textual challenges through its constituent datasets.

The bounding-boxes in the dataset are derived from the works of Shao et al. [47] and Wang et al. [62]. We employed GPT-4o, one of the state-of-the-art models, for image captioning. Following this process, we conducted manual quality review and refinement, and further integrated the VQA-Verify dataset. A more detailed description of the datasets is provided in Appendix C.

5 Experiments

5.1 Implementation

Our model is based on the Qwen2.5-VL-Instruct-3B backbone. We perform direct RL training using the framework introduced in [81] without any cold start. The training approach adopts the well-known GRPO-zero [48] method, with the reward function aligned with that of Section 3. For training data, we use the lightweight VQA-Verify dataset proposed earlier in Section 4. The model uses a configuration of $256 \times 28 \times 28$ as the min pixel setting and $512 \times 28 \times 28$ as the max pixel setting. The evaluation is conducted under the same settings. We set GRPO-3B as the baseline, which uses the same dataset but does not incorporate BBox or Caption rewards. Its reasoning format follows the original R1-like free-form reasoning, namely, "think first, then answer." More implementation details could be found in Appendix E.

For evaluation, we primarily rely on several comprehensive benchmarks: MMBench [29], MMStar [5], MME [11] and OCRBench [31]. We also compare our method with the current state-of-the-art reasoning models on three mathematical datasets: MathVista [34], Math-V [61], and MathVerse [78]. Results are presented in Table 1, Table 2 and Figure 5.

5.2 Main Results

As shown in Table 1, SATORI achieves substantial improvements across most sub-tasks. The overall average accuracy increases from 60.8% (original Qwen2.5-VL-Instruct-3B) to 76.5%, marking a gain of 15.7 percentage points. Compared to the free-form reasoning approach, which achieves 64.6%, SATORI improves by 11.9 percentage points. A closer look at individual metrics reveals that in the Fine-grained Perception (FP-S) sub-task "Object Localization," SATORI boosts performance from 40.0% to 60.0%. Even in more challenging tasks such as Logical Reasoning (LR) and Relational Reasoning (RR), SATORI maintains a lead—for instance, improving accuracy on "Social Relation" from 56.0% to 62.0%, and on "Nature Relation" from 56.8% to 58.1%. These results strongly demonstrate the effectiveness of our reasoning patterns in enhancing vision–language alignment and fine-grained understanding.

In Table 2, we can see that our SATORI-3B consistently narrows the gap between smaller open-source reasoners and much larger closed-source systems. On MathVista, SATORI-3B attains 60.9%, improving by over 9 points compared to the next best 2–3B model (R1-VL-2B). Likewise, on the more challenging Math-V and MathVerse datasets, SATORI-3B outperforms R1-VL-2B by 4.6 and 6.0 points, respectively. On the MMStar benchmark, SATORI-3B achieves 55.9%, matching the performance of several larger 8–11B reasoning models. In Figure 5, SATORI consistently outperforms the original Qwen2.5-VL-Instruct-3B model as well as its free-form reasoning variant on the MME dataset’s Reasoning, Code Reasoning, and Commonsense Reasoning tasks, as well as on OCRBench, demonstrating the superiority of our approach.

Table 1: **Comparison of SATORI with other MLLMs and methods in MMBench [29].** SATORI outperforms other open-source models, surpasses alternative reasoning-based MLLM approaches, and achieves competitive performance across most benchmarks. Specifically, LR denotes Logical Reasoning, AR denotes Attribute Reasoning, RR denotes Relation Reasoning, PPR denotes Physical Property Reasoning, SITU represents Structuralized Image-Text Understanding, FP-C represents Fine-grained Perception (Cross Instance), FP-S represents Fine-grained Perception (Single Instance), and CP refers to Coarse Perception. Results marked with † are sourced from [10].

Model/Method	FP-S				FP-C			CP					AR			LR		RR			Avg.
	Action Recognition	Object Localization	Celebrity Recognition	OCR	Spatial Relationship	Attribute Comparison	Attribute Recognition	Image Emotion	Image Quality	Image Scene	Image Style	Image Topic	Function Reasoning	Identity Reasoning	PPR	Future Prediction	SITU	Nature Relation	Physical Relation	Social Relation	
GPT-4V†	73.5	36.2	61.2	93.3	44.0	46.7	78.7	56.7	37.9	81.9	76.1	94.4	88.9	96.1	53.2	65.3	56.0	68.5	33.3	64.8	65.4
Gemini-1.5 Pro†	85.5	69.5	84.4	77.8	66.7	65.3	93.3	74.4	49.2	84.7	79.3	75.6	85.6	94.7	64.6	61.3	65.1	83.7	52	69.2	74.6
Gemini-2.0 Flash†	86.3	66.7	72.1	74.4	65.3	78.7	70.8	64.4	54.0	74.3	65.2	78.9	80.0	78.9	60.8	64.0	63.3	79.3	50.7	75.8	70.4
Llava-Next-8B†	80.3	64.8	74.8	83.3	44.0	66.7	79.8	78.9	48.4	85.4	79.3	97.8	88.9	97.4	64.6	66.7	37.6	66.3	50.7	84.6	72.1
Llava-CoT-11B†	81.2	62.9	89.1	92.2	48	62.7	86.5	74.4	46.8	83.3	75.0	88.9	90.0	98.7	67.1	66.7	49.5	79.3	56.0	82.4	74.4
<i>Qwen2.5-VL-Ins-3B</i>																					
Original	78.2	40.0	66.7	70.0	22.0	29.4	56.7	81.7	21.4	89.6	59.7	76.7	83.3	96.1	41.5	42.0	45.9	66.1	40.0	88.7	60.8
GRPO-3B	76.9	52.9	94.9	75.0	38.0	27.5	86.7	81.7	39.3	56.2	83.9	43.3	86.7	98.0	34.0	42.0	56.8	56.5	56.0	85.5	64.6
SATORI-3B	83.3	60.0	97.0	91.7	46.0	66.7	90.0	88.3	38.1	93.8	82.3	91.7	86.7	98.0	52.8	54.0	58.1	80.6	62.0	91.9	76.5

Table 2: Comparison with other reasoning models on three mathematical datasets (MathVista [34], Math-V [61], MathVerse [78]) and MMStar [5]. The results indicate that our method also maintains competitive performance on mathematical problems.

Method	MathVista	Math-V	MathVerse	MMStar
<i>Closed-Source Model</i>				
GPT-4o [18]	63.8	30.3	39.4	63.8
Claude-3.5 Sonnet [1]	67.7	38.0	-	62.2
<i>8-11B Reasoning Model</i>				
MultiMath-7B [42]	50.0	-	26.9	-
LLaVA-CoT-11B [68]	54.8	-	-	57.6
LLaVA-Reasoner-8B [79]	50.6	-	-	54.0
Insight-V-8B [8]	49.8	-	-	57.6
<i>2-3B Reasoning Model</i>				
Mulberry-2B [70]	51.7	-	-	51.3
R1-VL-2B [76]	52.1	17.1	26.2	49.8
Aquila-VL-2B [13]	59.0	18.4	26.2	54.9
SATORI-3B	60.9	21.7	32.2	55.9

5.3 Analysis

Ablation Study on Reasoning Patterns.

To validate the effectiveness of each component in SATORI, we compare the model’s performance under different reward configurations: using BBox without Caption, using neither, and supervised fine-tuning. All experiments were conducted on the same VQA-Verify dataset introduced in Section 4, with hyperparameter settings consistent with those described in Appendix E. The only differences lie in the training strategies and the choice of reward signals.

The results in Table 3 demonstrate that our method achieves the best performance when both BBox and Caption reward signals are present.

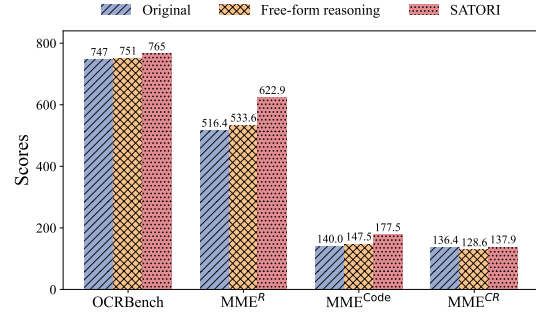


Figure 5: Performance of different methods across various reasoning and OCR benchmarks. Specifically, MME^R denotes the Reasoning subtask of MME [11], MME^{Code} denotes Code Reasoning subtask and MME^{CR} denotes Commonsense Reasoning subtask.

Table 3: Ablation results on reasoning patterns.

Method	MMBench	MMStar
Qwen2.5-VL-Ins-3B	60.8	48.0
+BBox+SFT	58.9	49.7
+BBox+Caption+SFT	65.2	50.5
+Free Form Reasoning+RL	64.6	50.4
+BBox+RL	71.0	54.1
SATORI	76.5	55.9

Are Captions Really Needed? In our method, employing image captions as the reward signal introduces additional reasoning overhead. To address concerns about the issues above, we conducted an ablation in which the model is trained with the *BBox-Answer-Caption* sequence but, at inference time, stops generation immediately after the answer token. We refer to this variant as *SATORI-Reverse*. Table 4 summarizes the comparison between the original SATORI (*Caption-BBox-Answer*), SATORI-Reverse, and a baseline using only the bounding-box reward (BBox-only RL).

Table 4: Comparison of SATORI, SATORI-Reverse, and BBox-only RL paradigms.

Method	MMBench	MMStar	MME ^R	Avg. Len.
SATORI (Cap-BBox-Ans)	76.5	55.9	622.9	686.24
SATORI-Reverse (BBox-Ans-Cap)	75.9	55.7	549.6	79.22
BBox-only RL	71.0	54.1	526.1	59.10

Although SATORI-Reverse incurs the same training overhead, since captions are still generated and scored during RL, the inference-time token consumption drops by roughly 88.46% compared to SATORI (79.22 vs. 686.24 length on average). More importantly, the accuracy of SATORI-Reverse decreases by less than 1% compared to SATORI on both MMBench and MMStar, confirming that delaying caption generation to the final step does not hurt model focus or performance. These results validate that the caption-based reward is not only helpful for grounding visual attention and reducing gradient variance but also flexible in deployment: by reversing the output order, one can retain nearly identical performance while substantially reducing inference costs.

Variance Reduction Analysis. As shown in Figure 6a, SATORI exhibits substantially lower gradient variance compared to free-form reasoning baselines. The average variance during training drops from 0.025 to 0.018, representing a 27% reduction. This suggests that verifiable intermediate rewards act as variance-reducing control signals, enabling more stable and efficient policy learning. Moreover, the gradient-norm curves in Figure 6b show that SATORI converges in fewer steps, confirming that variance reduction translates directly into faster training.

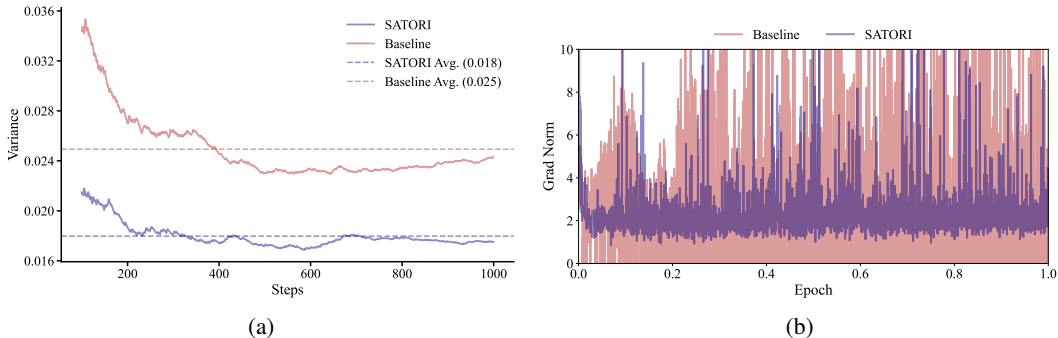


Figure 6: **a)** Comparison of SATORI with the classic free-form reasoning approach reveals the variance in GRPO performance. **b)** Changes in gradient norm over training epochs. The results show that our method converges significantly faster than free-form reasoning.

6 Conclusion

In this paper, we present SATORI, a staged optimization framework for visual reasoning tasks that integrates hierarchical intermediate supervision via three steps: caption generation, object localization, and final answer prediction. This design enables more verifiable and spatially grounded reasoning, and improves both learning efficiency and model robustness. To support this method, we construct VQA-Verify, a dataset with 12k annotated examples, enabling reward decomposition for reinforcement learning without extra models or manual reward engineering. Extensive experiments across multiple benchmarks demonstrate consistent performance gains, highlighting the effectiveness of intermediate supervision signals in guiding multi-modal models. Overall, this work sheds light on how spatial anchoring and intermediate supervision can be effectively combined with reinforcement learning to enhance multi-modal reasoning.

References

- [1] Anthropic. Claude 3.5 sonnet, 2024. URL <https://www.anthropic.com/news/claude-3-5-sonnet>.
- [2] Jinze Bai, Shuai Bai, Shusheng Yang, Shijie Wang, Sinan Tan, Peng Wang, Junyang Lin, Chang Zhou, and Jingren Zhou. Qwen-vl: A frontier large vision-language model with versatile abilities. *arXiv preprint arXiv:2308.12966*, 1(2):3, 2023.
- [3] Yuntao Bai, Andy Jones, Kamal Ndousse, Amanda Askell, Anna Chen, Nova DasSarma, Dawn Drain, Stanislav Fort, Deep Ganguli, Tom Henighan, et al. Training a helpful and harmless assistant with reinforcement learning from human feedback. *arXiv preprint arXiv:2204.05862*, 2022.
- [4] Soravit Changpinyo, Doron Kukliansy, Idan Szpektor, Xi Chen, Nan Ding, and Radu Soricut. All you may need for vqa are image captions. In *Proceedings of the 2022 Conference of the North American Chapter of the Association for Computational Linguistics: Human Language Technologies*, pages 1947–1963, 2022.
- [5] Lin Chen, Jinsong Li, Xiaoyi Dong, Pan Zhang, Yuhang Zang, Zehui Chen, Haodong Duan, Jiaqi Wang, Yu Qiao, Dahua Lin, et al. Are we on the right way for evaluating large vision-language models? *arXiv preprint arXiv:2403.20330*, 2024.
- [6] Zesen Cheng, Sicong Leng, Hang Zhang, Yifei Xin, Xin Li, Guanzheng Chen, Yongxin Zhu, Wenqi Zhang, Ziyang Luo, Deli Zhao, et al. Videollama 2: Advancing spatial-temporal modeling and audio understanding in video-llms. *arXiv preprint arXiv:2406.07476*, 2024.
- [7] Chee-Kheng Ch'ng, Chee Seng Chan, and Cheng-Lin Liu. Total-text: toward orientation robustness in scene text detection. *International Journal on Document Analysis and Recognition (IJDAR)*, 23(1):31–52, 2020.
- [8] Yuhao Dong, Zuyan Liu, Hai-Long Sun, Jingkang Yang, Winston Hu, Yongming Rao, and Ziwei Liu. Insight-v: Exploring long-chain visual reasoning with multimodal large language models. *arXiv preprint arXiv:2411.14432*, 2024.
- [9] Alexey Dosovitskiy, Lucas Beyer, Alexander Kolesnikov, Dirk Weissenborn, Xiaohua Zhai, Thomas Unterthiner, Mostafa Dehghani, Matthias Minderer, Georg Heigold, Sylvain Gelly, et al. An image is worth 16x16 words: Transformers for image recognition at scale. *arXiv preprint arXiv:2010.11929*, 2020.
- [10] Haodong Duan, Junming Yang, Yuxuan Qiao, Xinyu Fang, Lin Chen, Yuan Liu, Xiaoyi Dong, Yuhang Zang, Pan Zhang, Jiaqi Wang, et al. Vlmevalkit: An open-source toolkit for evaluating large multi-modality models. In *Proceedings of the 32nd ACM international conference on multimedia*, pages 11198–11201, 2024.
- [11] Chaoyou Fu, Peixian Chen, Yunhang Shen, Yulei Qin, Mengdan Zhang, Xu Lin, Jinrui Yang, Xiawu Zheng, Ke Li, Xing Sun, Yunsheng Wu, and Rongrong Ji. Mme: A comprehensive evaluation benchmark for multimodal large language models, 2024. URL <https://arxiv.org/abs/2306.13394>.
- [12] Aaron Grattafiori, Abhimanyu Dubey, Abhinav Jauhri, Abhinav Pandey, Abhishek Kadian, Ahmad Al-Dahle, Aiesha Letman, Akhil Mathur, Alan Schelten, Alex Vaughan, et al. The llama 3 herd of models. *arXiv preprint arXiv:2407.21783*, 2024.
- [13] Shuhao Gu, Jialing Zhang, Siyuan Zhou, Kevin Yu, and etc. Infinity-mm: Scaling multimodal performance with large-scale and high-quality instruction data, 2025. URL <https://arxiv.org/abs/2410.18558>.
- [14] Daya Guo, Dejian Yang, Haowei Zhang, Junxiao Song, Ruoyu Zhang, Runxin Xu, Qihao Zhu, Shirong Ma, Peiyi Wang, Xiao Bi, et al. Deepseek-r1: Incentivizing reasoning capability in llms via reinforcement learning. *arXiv preprint arXiv:2501.12948*, 2025.

- [15] Alex Havrilla, Yuqing Du, Sharath Chandra Raparthy, Christoforos Nalmpantis, Jane Dwivedi-Yu, Maksym Zhuravinskyi, Eric Hambro, Sainbayar Sukhbaatar, and Roberta Raileanu. Teaching large language models to reason with reinforcement learning. *arXiv preprint arXiv:2403.04642*, 2024.
- [16] Zheng Huang, Kai Chen, Jianhua He, Xiang Bai, Dimosthenis Karatzas, Shijian Lu, and CV Jawahar. Icdar2019 competition on scanned receipt ocr and information extraction. In *2019 International Conference on Document Analysis and Recognition (ICDAR)*, pages 1516–1520. IEEE, 2019.
- [17] Drew A Hudson and Christopher D Manning. Gqa: A new dataset for real-world visual reasoning and compositional question answering. In *Proceedings of the IEEE/CVF conference on computer vision and pattern recognition*, pages 6700–6709, 2019.
- [18] Aaron Hurst, Adam Lerer, Adam P Goucher, Adam Perelman, Aditya Ramesh, Aidan Clark, AJ Ostrow, Akila Welihinda, Alan Hayes, Alec Radford, et al. Gpt-4o system card. *arXiv preprint arXiv:2410.21276*, 2024.
- [19] Leslie Pack Kaelbling, Michael L Littman, and Andrew W Moore. Reinforcement learning: A survey. *Journal of artificial intelligence research*, 4:237–285, 1996.
- [20] Dimosthenis Karatzas, Faisal Shafait, Seiichi Uchida, Masakazu Iwamura, Lluís Gomez i Bigorda, Sergi Robles Mestre, Joan Mas, David Fernandez Mota, Jon Almazan Almazan, and Lluís Pere De Las Heras. Icdar 2013 robust reading competition. In *2013 12th international conference on document analysis and recognition*, pages 1484–1493. IEEE, 2013.
- [21] Dimosthenis Karatzas, Lluís Gomez-Bigorda, Anguelos Nicolaou, Suman Ghosh, Andrew Bagdanov, Masakazu Iwamura, Jiri Matas, Lukas Neumann, Vijay Ramaseshan Chandrasekhar, Shijian Lu, et al. Icdar 2015 competition on robust reading. In *2015 13th international conference on document analysis and recognition (ICDAR)*, pages 1156–1160. IEEE, 2015.
- [22] Timo Kaufmann, Paul Weng, Viktor Bengs, and Eyke Hüllermeier. A survey of reinforcement learning from human feedback. *arXiv preprint arXiv:2312.14925*, 10, 2023.
- [23] Alina Kuznetsova, Hassan Rom, Neil Alldrin, Jasper Uijlings, Ivan Krasin, Jordi Pont-Tuset, Shahab Kamali, Stefan Popov, Matteo Mallocci, Alexander Kolesnikov, et al. The open images dataset v4: Unified image classification, object detection, and visual relationship detection at scale. *International journal of computer vision*, 128(7):1956–1981, 2020.
- [24] Xiang Lan, Feng Wu, Kai He, Qinghao Zhao, Shenda Hong, and Mengling Feng. Gem: Empowering mllm for grounded eeg understanding with time series and images. *arXiv preprint arXiv:2503.06073*, 2025.
- [25] Chunyuan Li, Cliff Wong, Sheng Zhang, Naoto Usuyama, Haotian Liu, Jianwei Yang, Tristan Naumann, Hoifung Poon, and Jianfeng Gao. Llava-med: Training a large language-and-vision assistant for biomedicine in one day. *arXiv preprint arXiv:2306.00890*, 2023.
- [26] Fangyu Liu, Guy Emerson, and Nigel Collier. Visual spatial reasoning. *Transactions of the Association for Computational Linguistics*, 11:635–651, 2023.
- [27] Haotian Liu, Chunyuan Li, Yuheng Li, Bo Li, Yuanhan Zhang, Sheng Shen, and Yong Jae Lee. Llava-next: Improved reasoning, ocr, and world knowledge, January 2024. URL <https://llava-vl.github.io/blog/2024-01-30-llava-next/>.
- [28] Haotian Liu, Chunyuan Li, Qingyang Wu, and Yong Jae Lee. Visual instruction tuning. *Advances in neural information processing systems*, 36, 2024.
- [29] Yuan Liu, Haodong Duan, Yuanhan Zhang, Bo Li, Songyang Zhang, Wangbo Zhao, Yike Yuan, Jiaqi Wang, Conghui He, Ziwei Liu, et al. Mmbench: Is your multi-modal model an all-around player? In *European conference on computer vision*, pages 216–233. Springer, 2024.
- [30] Yuliang Liu, Lianwen Jin, Shuaitao Zhang, Canjie Luo, and Sheng Zhang. Curved scene text detection via transverse and longitudinal sequence connection. *Pattern Recognition*, 90: 337–345, 2019.

- [31] Yuliang Liu, Zhang Li, Mingxin Huang, Biao Yang, Wenwen Yu, Chunyuan Li, Xu-Cheng Yin, Cheng-Lin Liu, Lianwen Jin, and Xiang Bai. Ocrbench: on the hidden mystery of ocr in large multimodal models. *Science China Information Sciences*, 67(12):220102, 2024.
- [32] Yuliang Liu, Biao Yang, Qiang Liu, Zhang Li, Zhiyin Ma, Shuo Zhang, and Xiang Bai. Textmonkey: An ocr-free large multimodal model for understanding document. *arXiv preprint arXiv:2403.04473*, 2024.
- [33] Ziyu Liu, Zeyi Sun, Yuhang Zang, Xiaoyi Dong, Yuhang Cao, Haodong Duan, Dahua Lin, and Jiaqi Wang. Visual-rft: Visual reinforcement fine-tuning. *arXiv preprint arXiv:2503.01785*, 2025.
- [34] Pan Lu, Hritik Bansal, Tony Xia, Jiacheng Liu, Chunyuan Li, Hannaneh Hajishirzi, Hao Cheng, Kai-Wei Chang, Michel Galley, and Jianfeng Gao. Mathvista: Evaluating mathematical reasoning of foundation models in visual contexts. *arXiv preprint arXiv:2310.02255*, 2023.
- [35] Trung Quoc Luong, Xinbo Zhang, Zhanming Jie, Peng Sun, Xiaoran Jin, and Hang Li. Rft: Reasoning with reinforced fine-tuning. *arXiv preprint arXiv:2401.08967*, 2024.
- [36] Chenyang Lyu, Minghao Wu, Longyue Wang, Xinting Huang, Bingshuai Liu, Zefeng Du, Shuming Shi, and Zhaopeng Tu. Macaw-llm: Multi-modal language modeling with image, audio, video, and text integration. *arXiv preprint arXiv:2306.09093*, 2023.
- [37] Harry Markowitz. Portfolio selection. *The Journal of Finance*, 7(1):77–91, 1952.
- [38] Minesh Mathew, Dimosthenis Karatzas, and CV Jawahar. Docvqa: A dataset for vqa on document images. In *Proceedings of the IEEE/CVF winter conference on applications of computer vision*, pages 2200–2209, 2021.
- [39] Minesh Mathew, Viraj Bagal, Rubèn Tito, Dimosthenis Karatzas, Ernest Valveny, and CV Jawahar. Infographicvqa. In *Proceedings of the IEEE/CVF Winter Conference on Applications of Computer Vision*, pages 1697–1706, 2022.
- [40] Nibal Nayef, Yash Patel, Michal Busta, Pinaki Nath Chowdhury, Dimosthenis Karatzas, Wafa Khlif, Jiri Matas, Umapada Pal, Jean-Christophe Burie, Cheng-lin Liu, et al. Icdar2019 robust reading challenge on multi-lingual scene text detection and recognition—rrc-mlt-2019. In *2019 International conference on document analysis and recognition (ICDAR)*, pages 1582–1587. IEEE, 2019.
- [41] OpenAI. Introducing openai o1, 2024. URL <https://openai.com/o1/>.
- [42] Shuai Peng, Di Fu, Liangcai Gao, Xiuqin Zhong, Hongguang Fu, and Zhi Tang. Multi-math: Bridging visual and mathematical reasoning for large language models. *arXiv preprint arXiv:2409.00147*, 2024.
- [43] Xiaoye Qu, Jiashuo Sun, Wei Wei, and Yu Cheng. Look, compare, decide: Alleviating hallucination in large vision-language models via multi-view multi-path reasoning. *arXiv preprint arXiv:2408.17150*, 2024.
- [44] Xiaoye Qu, Yafu Li, Zhaochen Su, Weigao Sun, Jianhao Yan, Dongrui Liu, Ganqu Cui, Daizong Liu, Shuxian Liang, Junxian He, et al. A survey of efficient reasoning for large reasoning models: Language, multimodality, and beyond. *arXiv preprint arXiv:2503.21614*, 2025.
- [45] Rafael Rafailov, Archit Sharma, Eric Mitchell, Christopher D Manning, Stefano Ermon, and Chelsea Finn. Direct preference optimization: Your language model is secretly a reward model. *Advances in Neural Information Processing Systems*, 36:53728–53741, 2023.
- [46] John Schulman, Filip Wolski, Prafulla Dhariwal, Alec Radford, and Oleg Klimov. Proximal policy optimization algorithms. *arXiv preprint arXiv:1707.06347*, 2017.
- [47] Hao Shao, Shengju Qian, Han Xiao, Guanglu Song, Zhuofan Zong, Letian Wang, Yu Liu, and Hongsheng Li. Visual cot: Advancing multi-modal language models with a comprehensive dataset and benchmark for chain-of-thought reasoning. *Advances in Neural Information Processing Systems*, 37:8612–8642, 2024.

- [48] Zhihong Shao, Peiyi Wang, Qihao Zhu, Runxin Xu, Junxiao Song, Xiao Bi, Haowei Zhang, Mingchuan Zhang, YK Li, Y Wu, et al. Deepseekmath: Pushing the limits of mathematical reasoning in open language models. *arXiv preprint arXiv:2402.03300*, 2024.
- [49] Oleksii Sidorov, Ronghang Hu, Marcus Rohrbach, and Amanpreet Singh. Textcaps: a dataset for image captioning with reading comprehension. In *Computer Vision–ECCV 2020: 16th European Conference, Glasgow, UK, August 23–28, 2020, Proceedings, Part II 16*, pages 742–758. Springer, 2020.
- [50] Amanpreet Singh, Vivek Natarajan, Meet Shah, Yu Jiang, Xinlei Chen, Dhruv Batra, Devi Parikh, and Marcus Rohrbach. Towards vqa models that can read. In *Proceedings of the IEEE/CVF conference on computer vision and pattern recognition*, pages 8317–8326, 2019.
- [51] Zhaochen Su, Jun Zhang, Tong Zhu, Xiaoye Qu, Juntao Li, Min Zhang, and Yu Cheng. Timo: Towards better temporal reasoning for language models. *arXiv preprint arXiv:2406.14192*, 2024.
- [52] Zhaochen Su, Linjie Li, Mingyang Song, Yunzhuo Hao, Zhengyuan Yang, Jun Zhang, Guanjie Chen, Jiawei Gu, Juntao Li, Xiaoye Qu, et al. Openthinking: Learning to think with images via visual tool reinforcement learning. *arXiv preprint arXiv:2505.08617*, 2025.
- [53] Guangzhi Sun, Wenyi Yu, Changli Tang, Xianzhao Chen, Tian Tan, Wei Li, Lu Lu, Zejun Ma, Yuxuan Wang, and Chao Zhang. video-salmonn: Speech-enhanced audio-visual large language models. *arXiv preprint arXiv:2406.15704*, 2024.
- [54] Yipeng Sun, Jiaming Liu, Wei Liu, Junyu Han, Errui Ding, and Jingtuo Liu. Chinese street view text: Large-scale chinese text reading with partially supervised learning. In *Proceedings of the IEEE/CVF International Conference on Computer Vision*, pages 9086–9095, 2019.
- [55] Kimi Team, Angang Du, Bofei Gao, Bowei Xing, Changjiu Jiang, Cheng Chen, Cheng Li, Chenjun Xiao, Chenzhuang Du, Chonghua Liao, et al. Kimi k1. 5: Scaling reinforcement learning with llms. *arXiv preprint arXiv:2501.12599*, 2025.
- [56] Omkar Thawakar, Dinura Dissanayake, Ketan More, Ritesh Thawkar, Ahmed Heakl, Noor Ahsan, Yuhao Li, Mohammed Zumri, Jean Lahoud, Rao Muhammad Anwer, et al. Llamav-o1: Rethinking step-by-step visual reasoning in llms. *arXiv preprint arXiv:2501.06186*, 2025.
- [57] Jordy Van Landeghem, Rubèn Tito, Łukasz Borchmann, Michał Pietruszka, Paweł Joziak, Rafał Powalski, Dawid Jurkiewicz, Mickaël Coustaty, Bertrand Anckaert, Ernest Valveny, et al. Document understanding dataset and evaluation (dude). In *Proceedings of the IEEE/CVF International Conference on Computer Vision*, pages 19528–19540, 2023.
- [58] Andreas Veit, Tomas Matera, Lukas Neumann, Jiri Matas, and Serge Belongie. Coco-text: Dataset and benchmark for text detection and recognition in natural images. *arXiv preprint arXiv:1601.07140*, 2016.
- [59] Catherine Wah, Steve Branson, Peter Welinder, Pietro Perona, and Serge Belongie. The caltech-ucsd birds-200-2011 dataset. 2011.
- [60] Jiaan Wang, Fandong Meng, Yunlong Liang, and Jie Zhou. Drt-o1: Optimized deep reasoning translation via long chain-of-thought. *arXiv e-prints*, pages arXiv–2412, 2024.
- [61] Ke Wang, Junting Pan, Weikang Shi, Zimu Lu, Houxing Ren, Aojun Zhou, Mingjie Zhan, and Hongsheng Li. Measuring multimodal mathematical reasoning with math-vision dataset. *Advances in Neural Information Processing Systems*, 37:95095–95169, 2024.
- [62] Xinyu Wang, Yuliang Liu, Chunhua Shen, Chun Chet Ng, Canjie Luo, Lianwen Jin, Chee Seng Chan, Anton van den Hengel, and Liangwei Wang. On the general value of evidence, and bilingual scene-text visual question answering. In *Proceedings of the IEEE/CVF Conference on Computer Vision and Pattern Recognition*, pages 10126–10135, 2020.
- [63] Yaoting Wang, Shengqiong Wu, Yuecheng Zhang, Shuicheng Yan, Ziwei Liu, Jiebo Luo, and Hao Fei. Multimodal chain-of-thought reasoning: A comprehensive survey, 2025. URL <https://arxiv.org/abs/2503.12605>.

- [64] Christopher JCH Watkins and Peter Dayan. Q-learning. *Machine learning*, 8:279–292, 1992.
- [65] Mingrui Wu, Xinyue Cai, Jiayi Ji, Jiale Li, Oucheng Huang, Gen Luo, Hao Fei, Guannan Jiang, Xiaoshuai Sun, and Rongrong Ji. Controlmllm: Training-free visual prompt learning for multimodal large language models. *Advances in Neural Information Processing Systems*, 37: 45206–45234, 2024.
- [66] Shengqiong Wu, Hao Fei, Leigang Qu, Wei Ji, and Tat-Seng Chua. Next-gpt: Any-to-any multimodal llm. *arXiv preprint arXiv:2309.05519*, 2023.
- [67] Guowei Xu, Peng Jin, Li Hao, Yibing Song, Lichao Sun, and Li Yuan. Llava-o1: Let vision language models reason step-by-step. *arXiv preprint arXiv:2411.10440*, 2024.
- [68] Guowei Xu, Peng Jin, Li Hao, Yibing Song, Lichao Sun, and Li Yuan. Llava-o1: Let vision language models reason step-by-step. *arXiv preprint arXiv:2411.10440*, 2024.
- [69] Jianhao Yan, Yafu Li, Zican Hu, Zhi Wang, Ganqu Cui, Xiaoye Qu, Yu Cheng, and Yue Zhang. Learning to reason under off-policy guidance. *arXiv preprint arXiv:2504.14945*, 2025.
- [70] Huanjin Yao, Jiaying Huang, Wenhao Wu, Jingyi Zhang, Yibo Wang, Shunyu Liu, Yingjie Wang, Yuxin Song, Haocheng Feng, Li Shen, et al. Mulberry: Empowering mllm with o1-like reasoning and reflection via collective monte carlo tree search. *arXiv preprint arXiv:2412.18319*, 2024.
- [71] Jiabo Ye, Anwen Hu, Haiyang Xu, Qinghao Ye, Ming Yan, Yuhao Dan, Chenlin Zhao, Guohai Xu, Chenliang Li, Junfeng Tian, et al. mplug-docowl: Modularized multimodal large language model for document understanding. *arXiv preprint arXiv:2307.02499*, 2023.
- [72] Huaiyuan Ying, Shuo Zhang, Linyang Li, Zhejiang Zhou, Yunfan Shao, Zhaoye Fei, Yichuan Ma, Jiawei Hong, Kuikun Liu, Ziyi Wang, et al. Internlm-math: Open math large language models toward verifiable reasoning. *arXiv preprint arXiv:2402.06332*, 2024.
- [73] Qiyang Yu, Zheng Zhang, Ruofei Zhu, Yufeng Yuan, Xiaochen Zuo, Yu Yue, Tiantian Fan, Gaohong Liu, Lingjun Liu, Xin Liu, et al. Dapo: An open-source llm reinforcement learning system at scale. *arXiv preprint arXiv:2503.14476*, 2025.
- [74] Dan Zhang, Sining Zhoubian, Ziniu Hu, Yisong Yue, Yuxiao Dong, and Jie Tang. Rest-mcts*: Llm self-training via process reward guided tree search. *arXiv preprint arXiv:2406.03816*, 2024.
- [75] Jiarui Zhang, Mahyar Khayatkhoei, Prateek Chhikara, and Filip Ilievski. Mllms know where to look: Training-free perception of small visual details with multimodal llms. *arXiv preprint arXiv:2502.17422*, 2025.
- [76] Jingyi Zhang, Jiaying Huang, Huanjin Yao, Shunyu Liu, Xikun Zhang, Shijian Lu, and Dacheng Tao. R1-vl: Learning to reason with multimodal large language models via step-wise group relative policy optimization. *arXiv preprint arXiv:2503.12937*, 2025.
- [77] Jixiao Zhang and Chunsheng Zuo. Grpo-lead: A difficulty-aware reinforcement learning approach for concise mathematical reasoning in language models, 2025. URL <https://arxiv.org/abs/2504.09696>.
- [78] Renrui Zhang, Dongzhi Jiang, Yichi Zhang, Haokun Lin, Ziyu Guo, Pengshuo Qiu, Aojun Zhou, Pan Lu, Kai-Wei Chang, Yu Qiao, et al. Mathverse: Does your multi-modal llm truly see the diagrams in visual math problems? In *European Conference on Computer Vision*, pages 169–186. Springer, 2024.
- [79] Ruohong Zhang, Bowen Zhang, Yanghao Li, Haotian Zhang, Zhiqing Sun, Zhe Gan, Yinfei Yang, Ruoming Pang, and Yiming Yang. Improve vision language model chain-of-thought reasoning. *arXiv preprint arXiv:2410.16198*, 2024.
- [80] Xiaoman Zhang, Chaoyi Wu, Ziheng Zhao, Weixiong Lin, Ya Zhang, Yanfeng Wang, and Weidi Xie. Pmc-vqa: Visual instruction tuning for medical visual question answering. *arXiv preprint arXiv:2305.10415*, 2023.

- [81] Yuze Zhao, Jintao Huang, Jinghan Hu, Xingjun Wang, Yunlin Mao, Daoze Zhang, Zeyinzi Jiang, Zhikai Wu, Baole Ai, Ang Wang, et al. Swift: a scalable lightweight infrastructure for fine-tuning. In *Proceedings of the AAAI Conference on Artificial Intelligence*, volume 39, pages 29733–29735, 2025.
- [82] Yuke Zhu, Oliver Groth, Michael Bernstein, and Li Fei-Fei. Visual7w: Grounded question answering in images. In *Proceedings of the IEEE conference on computer vision and pattern recognition*, pages 4995–5004, 2016.

A Related Works

A.1 Enhancing Reasoning in MLLMs

Multimodal Large Language Models (MLLMs) have rapidly advanced the state of vision–language understanding by integrating text, image, and other sensory inputs. Early efforts primarily tackled image–text tasks, demonstrating the ability to generate descriptive captions and answer visual queries based on single-image prompts [28, 27, 43]. Subsequent research extended these models to video understanding [53, 6] and to more diverse modalities such as audio and point clouds [36, 66]. Domain-specific adaptations have further pushed the envelope: examples include specialized medical image interpretation [80, 25, 24] and structured document analysis [71, 32].

Building on the success of chain-of-thought prompting in pure-language settings [41], recent approaches seek to endow MLLMs with stronger inference capabilities via supervised fine-tuning on high-quality reasoning traces. Methods such as LLaVA-CoT generate structured intermediate reasoning steps—summary, description, analysis, conclusion—using a powerful teacher model and then train the target MLLM on these examples [67]. Other works incorporate search techniques: Mulberry employs a collective Monte Carlo Tree Search across multiple model instances to discover effective reasoning pathways, which are subsequently distilled into a single model [70].

A.2 Reinforcement Learning for Structured Reasoning

Reinforcement Learning (RL) provides a principled approach for sequential decision-making, where agents optimize long-term return through trial-and-error interactions [19, 64]. In the context of large language models, RL with human feedback (RLHF) has been instrumental in aligning generation quality to human preferences, using algorithms like PPO [46] and DPO [45] [3]. More recently, RL has been adopted to improve reasoning: ReST-MCTS* introduces a learned process reward model to evaluate intermediate reasoning steps [74], while other studies demonstrate that simple outcome-level rewards—assigning positive credit only to sequences that reach correct answers—are sufficient to guide policy optimization [35, 14, 55].

B Details of Visual Attention Map Comparison

B.1 Implementation

To ensure a fair comparison, we employed the original Qwen2.5-VL-Instruct-3B model to analyze visual attention maps under three different reasoning patterns, without any additional fine-tuning. The experiments were conducted on 2,000 randomly selected samples from the OpenImages [23] dataset.

Since the instruction-following capability of the 3B model is relatively limited, simply prompting it with a reasoning pattern may not guarantee adherence. Therefore, we adopted a one-shot example setting for comparative experiments. The prompts used in the experiments are as follows:

Prompt for Visual Attention Map Comparison

```
"ConventionalVQA":
# Output Example
Question: What is the capital city of France?
Answer: Paris
```

```

-----
"Free_Form_Reasoning":
Output the thinking process in <think> and
final answer in <answer> </answer> tags.

# Output Example
Question: What is the capital city of France?
<think>France is a country in Europe, and its capital city is Paris.
</think> <answer>Paris</answer>

-----

"Caption_BBox_Answer":
First, provide an image caption describing the overall scene inside
<caption> </caption>. Then, output the list of bounding-boxes in the
format of [[x1,y1,x2,y2], ...] inside <bbox> </bbox>. Finally, give
the final answer in <answer> </answer>.

# Output Example
Question: What is shown in the image?
<caption>A group of people playing soccer on a green field.</caption>
<bbox>[[50,60,120,180], [200,80,260,190], [300,90,360,200]]</bbox>
<answer>People are playing soccer.</answer>

```

B.2 Visual Attention Map Computation in MLLMs

Similar to the work of Zhang et al., when the model generates the n -th answer token during autoregressive decoding, we first extract the attention tensor across all layers and heads:

$$\mathbf{A} = [\text{softmax}(\frac{\mathbf{Q}_A \mathbf{K}^T}{\sqrt{d}})]_{L \times K} \in \mathbb{R}_+^{L \times K \times N_A \times N}, \tag{7}$$

where L is the number of layers, K is the number of heads per layer, N_A is the number of answer-token queries, and N is the total length of text and visual tokens. We then locate the start and end indices of the visual tokens in the input sequence, denoted `vs_pos` and `ve_pos`, and crop each layer-head attention to the visual embedding segment:

$$\mathbf{A}_I^{(\ell,k)} = \mathbf{A}_{n, \text{vs_pos:ve_pos}}^{(\ell,k)} \in \mathbb{R}_+^{N_A \times HW}, \tag{8}$$

where HW is the flattened spatial length of the visual patches. This segment is reshaped into a two-dimensional grid:

$$\mathbf{A}_I^{(\ell,k)} \xrightarrow{\text{reshape}} \mathbf{A}^{(\ell,k)} \in \mathbb{R}_+^{h \times w}, \tag{9}$$

with h and w denoting the number of patch rows and columns. To obtain a unified attention distribution, we average over all answer queries and attention heads:

$$\hat{\mathbf{A}} = \frac{1}{N_A K} \sum_{n=1}^{N_A} \sum_{k=1}^K \mathbf{A}^{(\ell,k)} \in \mathbb{R}_+^{h \times w}, \tag{10}$$

and normalize across the spatial dimensions to yield the final importance distribution:

$$\tilde{\mathbf{A}} = \text{Normalize}_{h,w}(\hat{\mathbf{A}}). \tag{11}$$

C Details of the Dataset

C.1 Caption Annotation

As stated previously in Section 4, the bounding-boxes used in our dataset are based on the annotations provided by Shao et al. [47] and Wang et al. [62]. For image captioning, we utilized GPT-4o, a cutting-edge model in the field. After generating captions, we carried out manual review and refinement to

ensure quality, and subsequently incorporated the VQA-Verify dataset into our work. The following prompt was used to generate caption annotations for the dataset.

Prompt for Caption Annotation

<image> Describe this image in general.

Examples of VQA-Verify are illustrated in Figure 7.

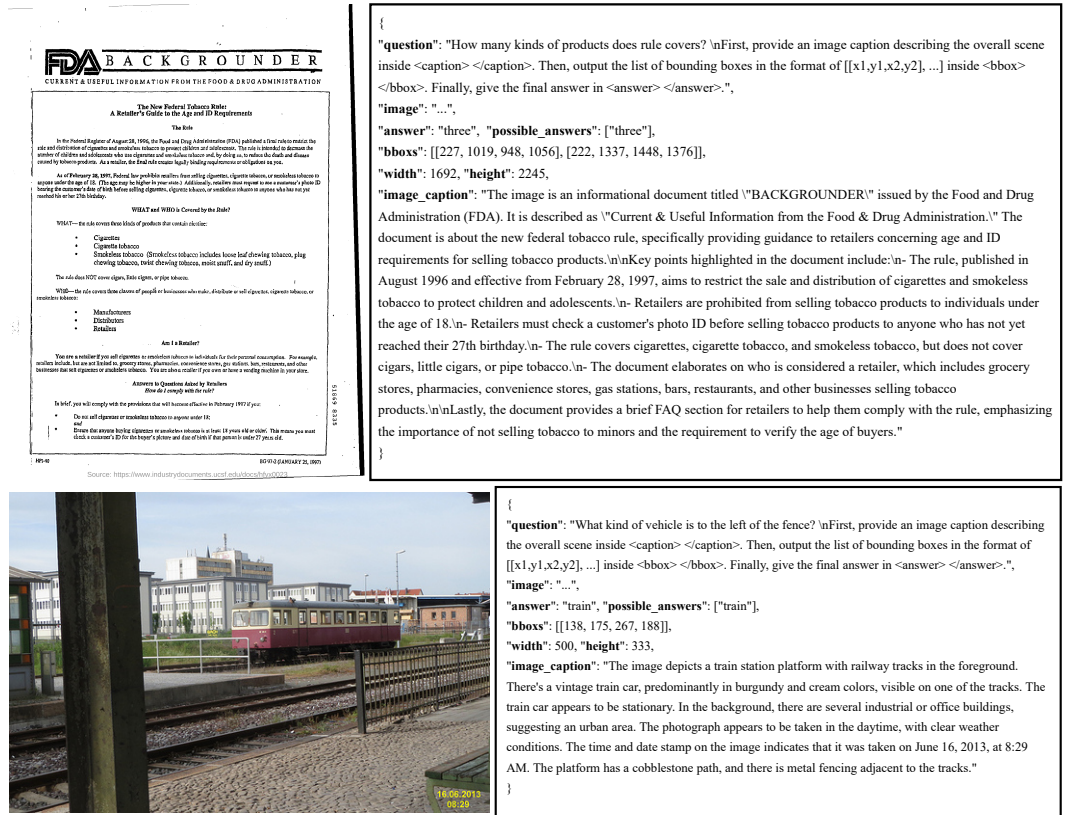


Figure 7: Examples of VQA-Verify.

C.2 Statics of VQA-Verify

Table 5 summarizes the overall size and annotation density of VQA-Verify, as well as the composition and average grounding signal per source dataset. The first row reports the total number of training samples, the average number of bounding-boxes per sample, and the average caption length in words. Subsequent rows break down these metrics for each of the integrated benchmark datasets, illustrating variation in visual complexity (boxes) and descriptive detail (caption length). The estvqa [62] dataset integrates data from Text-Total [7], ICDAR2013 [20], ICDAR2015 [21], CTW1500 [30], COCO-Text [58], LSVT [54], and MLT [40]. It is worth noting that the bounding-box annotations provided by Wang et al. are defined by four points rather than the standard rectangular format. To ensure consistency, we converted them to the common $[x_1, y_1, x_2, y_2]$ representation by computing the enclosing rectangle.

C.3 Dataset Verification

To ensure the quality of the automatically generated captions and bounding-boxes in VQA-Verify, we performed a manual verification on a sampled subset. Below we describe the verification procedure and summarize the results.

We randomly sampled 1,500 instances (12.5% of the 12,000 total samples) and conducted a manual review of each. During this review, captions were evaluated to ensure they accurately reflected

Source	# Samples	Avg BBoxes / Sample	Avg Caption Words
Train	12,000	1.34	112.12
cub-200 [59]	1,000	1.00	76.03
docvqa [38]	1,000	2.17	145.53
dude [57]	1,000	1.00	150.27
estvqa [62]	1,000	1.00	98.53
gqa [17]	1,000	1.00	86.53
infographicsvqa [39]	1,000	2.31	200.11
openimages [23]	1,000	1.00	81.27
sroie [16]	1,000	1.00	146.31
textcap [49]	1,000	1.84	96.93
textvqa [50]	1,000	1.72	95.77
v7w [82]	1,000	1.00	87.08
vsr [26]	1,000	1.00	80.97

Table 5: Overall and per-source statistics for VQA-Verify.

key image content, contained between 10 and 20 words, and were free from spelling or semantic errors; bounding-boxes were verified to tightly enclose the region relevant to the answer, with an Intersection-over-Union (IoU) of at least 0.8 relative to the original automatic annotation; and answers were checked for consistency with both the question and the image.

Item	Failures	Failure Rate	Common Issues
Caption Quality Check	27	1.8%	Overly verbose, missing details
bounding-box Accuracy Check	95	6.3%	Box misalignment, incomplete area
Answer Consistency Check	9	0.6%	Mismatch with image/question

Table 6: Summary of manual verification results.

D Supplementary Variance Analysis

To rigorously characterize the sources of policy gradient variance in GRPO, we leverage the *Law of Total Variance* to decouple the variance into intra-trajectory and inter-trajectory components. Let ∇J_{GRPO} denote the policy gradient estimator:

$$\nabla_{\theta} J_{\text{GRPO}} \approx \mathbb{E}_{q, o \sim \pi_{\theta_{\text{old}}}} \left[\frac{1}{G} \sum_{i=1}^G \frac{1}{|o_i|} \sum_{t=1}^{|o_i|} h_{i,t} \nabla_{\theta} \log \pi_{\theta}(o_{i,t} | q, o_{i,<t}) A_{i,t} \right] \quad (12)$$

In this expression, we omit the KL-divergence penalty and clipping terms from PPO since they are deterministic functions of the gradient and do not contribute to sampling noise. The *total variance* of the estimator can be decomposed as:

$$\text{Var}(\nabla J_{\text{GRPO}}) = \underbrace{\mathbb{E}_{\tau} [\text{Var}(\nabla J_{\text{GRPO}} | \tau)]}_{\text{Intra-Trajectory Variance}} + \underbrace{\text{Var}_{\tau} (\mathbb{E}[\nabla J_{\text{GRPO}} | \tau])}_{\text{Inter-Trajectory Variance}} \quad (13)$$

Here, τ denotes a sampled trajectory. The inter-trajectory term reflects variance due to differences in total rewards $R(\tau)$ across trajectories. In GRPO, the advantage at each token is normalized by the group statistics:

$$r_i = \frac{r_i - \text{mean}(\mathbf{r})}{\text{std}(\mathbf{r})}, \quad \mathbf{r} = \{r_i\}_{i=1}^G.$$

Thus the trajectory-conditional expected gradient scales as

$$\mathbb{E}[\nabla J_{\text{GRPO}} | \tau] \propto \frac{1}{|\mathcal{o}|} \sum_{t=1}^{|\mathcal{o}|} h_t g_t r_i, \quad g_{i,t} = \nabla_{\theta} \log \pi_{\theta}(o_{i,t} | q, o_{i,<t}). \quad (14)$$

Since trajectories are sampled independently but token generation within each trajectory is autoregressive, we have:

$$\text{Var}_{\tau}(\mathbb{E}[\nabla J_{\text{GRPO}} | \tau]) \propto \text{Var}(R(\tau)), \quad R(\tau) = \sum_{k=1}^n \beta_k R_k. \quad (15)$$

This shows that reducing the variance of the total reward $R(\tau)$ directly lowers the inter-trajectory variance and thus stabilizes gradient estimates.

Our observation in experiments shows that even though the verifiable reasoning patterns reward and the accuracy reward are often positively correlated, the overall variance of the total reward still decreases. This phenomenon can be explained by the *diversification effect* [37]: when the total reward is constructed as a weighted combination of multiple sub-rewards with weights $\{\beta_k\}$, the overall variance can be reduced even if the components are positively correlated.

According to the variance formula for a weighted sum:

$$\text{Var}(R(\tau)) = \sum_i \beta_i^2 \text{Var}(R_i) + 2 \sum_{i < j} \beta_i \beta_j \text{Cov}(R_i, R_j),$$

the total variance depends not only on the variances of the individual components but also on their pairwise covariances. Even when $\text{Cov}(R_i, R_j) > 0$, the squared weights $\beta_i^2 < 1$ for all i dilute the contribution of each term, and as long as the correlation coefficients $\rho_{ij} < 1$, the combined variance can be strictly smaller than the variance of a single reward term.

In the context of GRPO, the verifiable reasoning reward emphasizes consistency in intermediate reasoning steps (e.g., caption or bounding-box grounding), while the accuracy reward focuses on the final answer correctness. Although the two rewards are positively correlated, they capture complementary aspects of the task. By allocating appropriate weights, we retain useful signal from both while suppressing the noise associated with each individual component. This diversification not only reduces inter-trajectory variance but also leads to more stable gradient estimates and improved convergence behavior during training.

E Implementation Details

Our experiments are conducted using Qwen2.5-VL-Instruct-3B. The model’s MAX_PIXELS is set to $512 \times 28 \times 28$, and MIN_PIXELS to $256 \times 28 \times 28$. Training is performed on four NVIDIA H100 Tensor Core GPUs. For the dataset, we utilize VQA-Verify (see Section 4), which enables the incorporation of intermediate caption and bounding-box reward signals during training. In the reward configuration, we assign equal weight to all reward signals. That is, all values of β are set to $1/k$.

We do not perform a cold-start; instead, we train directly using GRPO. During training, we set max_length to 2048, and the GRPO group size G to 16, corresponding to a per-device batch size of 4. The sampling parameters are configured as follows: temperature = 1.0, top_k = 50, top_p = 0.9, and repetition_penalty = 1.0. We use a learning rate of 1×10^{-6} and perform full fine-tuning for one epoch. The clip range is set to 0.2, and the KL divergence coefficient to 0.05. Throughout training, only the linear layers are updated, while the visual encoder remains frozen. During training, we randomly selected 1% of the training set as the validation set.

F More Experiments

F.1 Detailed Results on MMStar

We present detailed comparative results on the MMStar dataset in Figure 8. The results show that our method consistently outperforms the 3B-GRPO baseline—which uses the same dataset and settings

but lacks verifiable signals—across all categories. Notably, on more complex reasoning and math tasks, SATORI surpasses it by more than 5%.

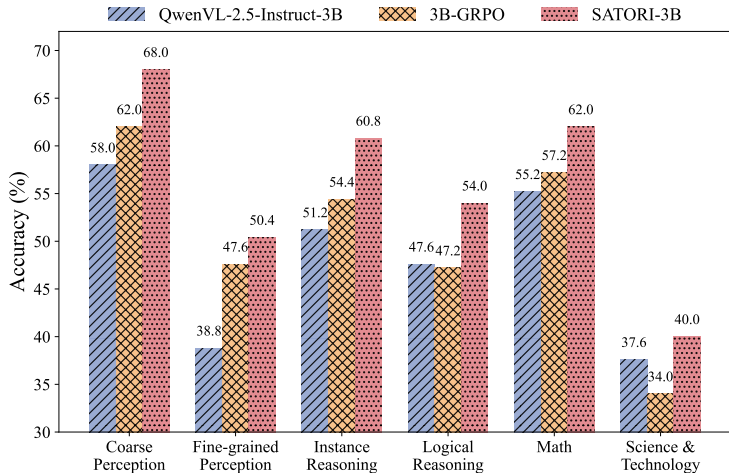


Figure 8: Comparison of model average performance on each category. SATORI outperforms the 3B-GRPO baseline, demonstrating the effectiveness of using verifiable reasoning patterns as rewards.

G Discussion

G.1 Limitations

Dependence on Base Model Instruction-Following and Grounding. While SATORI demonstrates significant benefits in zero-shot visual reasoning by leveraging a no-cold-start GRPO training scheme atop powerful base MLLMs, several limitations and avenues for future exploration remain. Our approach capitalizes on the strong instruction-following and visual grounding abilities of models such as Qwen2.5-VL. The ability to output bounding-boxes as intermediate rewards is a direct consequence of this pre-training on grounding tasks. However, for weaker base models that lack such capabilities, a purely zero-cold-start strategy may struggle. In these cases, an initial supervised fine-tuning (SFT) phase with task-specific data would likely be necessary to bootstrap both instruction adherence and structured reasoning. Similarly, models not pre-trained on visual grounding would benefit from a phase of visual-instruction tuning—exposing them to paired image, instruction, and bounding-box annotations—before applying our reinforcement framework.

Simplified Reasoning Paths in Standard VQA. Our experiments focus exclusively on standard VQA benchmarks, whose questions often admit relatively straightforward, single-step or shallow multi-step reasoning. Consequently, SATORI’s three-stage pipeline—caption, bbox, answer—suffices to guide the model effectively. Yet, real-world applications frequently demand deeper, branching reasoning, as exemplified by complex multi-modal mathematical problems. In such tasks, a single bounding-box per question does not adequately localize the multiple sub-regions pertinent to each reasoning step.

G.2 Future Works

Towards Fine-Grained, Step-by-Step Verification. Our future work will explore a more fine-grained verification framework in which, at each reasoning step, the model attends to and is rewarded on a distinct image region. By leveraging dynamic visual attention maps rather than a single bounding-box, we can decompose complex, multi-step problems—particularly in mathematics—into a sequence of visually grounded subtasks.

Adaptive Stage Decomposition and Model-Learned Structuring. Another promising direction is to move beyond a fixed three-stage pipeline toward models that learn their own optimal decomposition of tasks. By introducing a learnable stage controller, SATORI could adapt the number and nature of intermediate steps to each question’s complexity. Meta-learning or conditional computation

techniques may enable the model to decide, at inference time, how many reasoning sub-tasks are required and what form each should take (e.g., object detection, relation extraction, sub-captioning).